This is the author's peer reviewed, accepted manuscript. However, the online version of record will be different from this version once it has been copyedited and typeset

PLEASE CITE THIS ARTICLE AS DOI: 10.1063/5.0030215

### Magnetic Confinement of Effectively Unmagnetized Plasma Particles

C. A. Ordonez<sup>1,a</sup>
<sup>1</sup>Department of Physics,
University of North Texas,
Denton, Texas 76203, USA

(Dated: October 25, 2020)

### Abstract

A purely magnetic applied field may provide plasma confinement under conditions where the bulk of the plasma is effectively free of the applied magnetic field. The applied magnetic field surrounds the bulk of the plasma, and plasma particles that are incident on the applied magnetic field can be reflected back into the effectively unmagnetized region of plasma. The concept belongs to a class of magnetic plasma confinement approaches studied long ago, for which some experimental results indicated classical (collision-based) cross-magnetic-field transport may occur. However, multiple magnetic coils are required to be immersed within the confined plasma, and rapid plasma loss may occur if material structures are present that pass through the plasma (e.g., to hold the immersed coils in place). In the work reported, the concept is studied in combination with magnetic plasma expulsion [R. E. Phillips and C. A. Ordonez, Phys. Plasmas 25, 012508 (2018)], which would be employed to keep plasma away from material structures that pass through the plasma. A planar model is used for the study. A classical trajectory Monte Carlo simulation is carried out of particles that are independently incident on the applied magnetic field. With monoenergetic incident particles, the results indicate that the applied magnetic field can reflect all independently incident particles in certain regions of parameter space. Prospects for achieving three-dimensional magnetic confinement of an effectively unmagnetized plasma with a Maxwellian velocity distribution are discussed.

 $<sup>^{\</sup>rm a}$  Author to whom correspondence should be addressed. Electronic mail: cao@unt.edu.

### AIP Publishing

# This is the author's peer reviewed, accepted manuscript. However, the online version of record will be different from this version once it has been copyedited and typeset PLEASE CITE THIS ARTICLE AS DOI: 10.1063/5.0030215

### I. INTRODUCTION

An artificially structured boundary for plasma confinement is defined as a system of current carrying conductors and/or charged electrodes that produce a static electromagnetic field along the periphery of a confined plasma.<sup>1–5</sup> The bulk of the confined plasma would be effectively free of the applied electromagnetic field, and plasma confinement would occur as a result of particles being reflected from the applied field. An artificially structured boundary may serve to provide confinement along the edge of a nonneutral electron or positron plasma. An electric field is produced within an edge-confined nonneutral plasma, and a self-consistent Poisson-Boltzmann computation predicts that purely electric (plasma space-charge based) confinement of an ion plasma is possible.<sup>6</sup>

An artificially structured boundary that produces a combined magnetic and electric applied field has been studied using a classical trajectory Monte Carlo simulation. A spatially periodic magnetic field was considered to be produced by a planar sequence of parallel wires, with adjacent wires carrying currents in opposite directions. An electric field was superimposed to provide electrostatic plugging of a sequence of magnetic cusps associated with the magnetic field. The simulation indicated that the combined field can reflect all independently incident particles that follow a monoenergetic isotropic velocity distribution (i.e., arbitrarily oriented velocity vectors with the same magnitudes), in certain regions of parameter space, provided that all particles have the same sign of charge.

Plasma confinement with an artificially structured boundary has also been studied using a particle-in-cell simulation.<sup>3</sup> The artificially structured boundary was similar to the one described in Ref. 4, except that a nonplanar boundary enclosed an axisymmetric volume. The particle-in-cell simulation indicated that the enclosure may serve to confine a nonneutral plasma, in certain regions of parameter space.

An issue with using a combined magnetic and electric applied field for confining a nonneutral plasma is that the electric field produced by the plasma tends to reduce the effectiveness of the applied electric field. The effect may limit the density of the confined plasma. In the work reported here, an artificially structured boundary that produces a purely magnetic applied field is studied. Two sets of magnetic coils would be used, with one set of coils immersed within a confined plasma. It should be noted that, without the use of an applied electric field, confinement of a neutral plasma may be possible.

### AIP

This is the author's peer reviewed, accepted manuscript. However, the online version of record will be different from this version once it has been copyedited and typeset

PLEASE CITE THIS ARTICLE AS DOI: 10.1063/5.0030215

An artificially structured boundary that produces a purely magnetic applied field was studied in Refs. 1 and 2. The artificially structured boundary was considered to consist of one (or more) planar sequence of parallel wires, with adjacent wires in a plane carrying currents in opposite directions. The magnetic field was spatially periodic and produced a sequence of magnetic cusps. The magnetic field would reflect all independently incident charged particles only for a range of grazing angles of incidence, 1 and an approach for using an applied electric field for electrostatically plugging the magnetic cusps was discussed.<sup>2</sup> In contrast to the work presented here, the studies reported in Refs. 1 and 2 did not consider plasma-immersed components, and there was nothing to stop particles that would be incident normal to the plane of the artificially structured boundary and centered with a magnetic cusp from passing through the artificially structured boundary without being reflected. Similar to the work presented here, the studies reported in Refs. 1 and 2 employed a classical trajectory Monte Carlo simulation based on using normalized governing equations, such that the results would be more broadly applicable. The primary advancement that is reported here, beyond what was reported in Refs. 1 and 2, is a finding that simulated particles that are independently incident normal to the plane of an artificially structured boundary can all be reflected by a purely magnetic applied field in certain regions of parameter space, when plasma-immersed components are used.

Some early research indicates that classical (collision-based) cross-magnetic-field transport may occur in a class of magnetic plasma confinement approaches that employ multiple plasma-immersed magnetic coils, provided the effects of material structures that pass through the plasma are sufficiently small.<sup>7–12</sup> The magnetic plasma confinement approach studied here is of the same class and is characterized as having dimensions for the particle confinement volume that are large compared to the separation between adjacent plasma-immersed magnetic coils.

An issue with using plasma-immersed coils is that rapid plasma loss may occur if material structures are present that pass through the plasma (e.g., to hold the immersed coils in place). An artificial phenomenon referred to as magnetic plasma expulsion may serve to keep plasma away from material structures that connect to the plasma-immersed magnetic coils. <sup>13,14</sup> Research on the phenomenon using a particle-in-cell simulation was reported in Ref. 13. The possibility of fueling a magnetically confined plasma with particle sources located inside of the plasma within a magnetic expulsion field has been studied with a

This is the author's peer reviewed, accepted manuscript. However, the online version of record will be different from this version once it has been copyedited and typeset

PLEASE CITE THIS ARTICLE AS DOI: 10.1063/5.0030215

### AIP Publishing

classical trajectory Monte Carlo simulation.  $^{15}\,$ 

An artificially structured boundary may serve for confining or controlling plasma. There are many areas of scientific research that may benefit from the development of improved plasma confinement and control methods. For example, there are research groups that rely on plasma confinement and control methods for conducting research on antihydrogen. 16-20 With confinement of a sufficiently cold and dense nondrifting plasma that produces antihydrogen atoms, a relatively simple measurement to determine the direction of the gravitational acceleration of antimatter may be possible. 21 The use of multiple plasma-immersed coils was originally studied for confining a sufficiently hot and dense hydrogen-isotope plasma, such that fusion energy is produced. There are many types of plasma-based devices that have or can have multipolar magnetic fields (e.g., produced by permanent magnets) along a plasmafacing wall. Examples include the multipurpose device called the Big Red Ball, 22,23 high efficiency multistage plasma thrusters for space propulsion, <sup>24</sup> ion sources for charged particle beams.<sup>25</sup> plasma chambers for processing materials,<sup>26,27</sup> and other plasma confinement and control systems for studies of plasma phenomena.<sup>28-31</sup> Such devices may benefit from enhanced plasma confinement, which may be possible by incorporating plasma-immersed magnetic coils.

An example of a purely magnetic applied field that may serve for magnetic confinement of an effectively unmagnetized plasma is presented in Sec. II. The purely magnetic applied field would be produced by an artificially structured boundary consisting of axisymmetric magnetic coils. In Sec. III, a planar model of the artificially structured boundary is developed. The planar model is used in Sec. IV for finding simulated conditions under which independently incident particles are reflected by the applied field. The simulated conditions with magnetic plasma expulsion present are reported in Sec. V. A discussion is found in Sec. VI, and concluding remarks are in Sec. VII.

### II. AXISYMMETRIC CONFIGURATION

Figure 1 shows an example of a toroidal configuration that may serve for confining an effectively unmagnetized plasma with a purely magnetic applied field by using axisymmetric magnetic field coils. The plasma would be confined within an axisymmetric toroidal confinement volume. The configuration consists of two sets of axisymmetric magnetic coils of

# This is the author's peer reviewed, accepted manuscript. However, the online version of record will be different from this version once it has been copyedited and typeset PLEASE CITE THIS ARTICLE AS DOI: 10.1063/5.0030215

varying radii. A cylindrical coordinate system is defined with coordinates  $(r, \theta, z)$  and with the z axis coincident with the axis of symmetry of the configuration.

For the field shown in Fig. 1, the magnetic field of each coil is calculated as being produced by a single-turn circular current loop formed by an infinitesimally thin wire. A closed-form expression for the magnetic field  $\mathbf{B}_l(r,\theta,z)$  produced by such a current loop centered at the coordinate origin with radius  $R_k$  is obtained from Ref. 32. The magnetic field for a set of N loops evenly distributed on a toroidal surface with constant minor radius a and major radius R is given by

$$\boldsymbol{B}(r,\theta,z) = \sum_{k=1}^{N} \boldsymbol{B}_{l} \left[ r, \theta, z - a \cos \left( \frac{2\pi k}{N} \right) \right]$$
 (1)

with

$$R_k = R + a \sin\left(\frac{2\pi k}{N}\right),\tag{2}$$

where  $R_k$  is the radius of the kth circular current loop. For Fig. 1, the value N=12 is used for each of two sets of coils. Also, the dimensions are chosen such that a=1 for one set of coils and a=1.5 for the other set of coils. The value R=10 is used for both sets of coils.

The cross section of the confinement volume on an r-z plane is approximately circular for the configuration in Fig. 1. Other cross sectional shapes are also possible, such as rectangular, diamond and elliptical shapes.

### III. PLANAR MODEL

A planar model is developed for the artificially structured boundary shown in Fig. 1. The configuration consists of a number of straight parallel wires that are distributed evenly along two planes as shown in Fig. 2. A Cartesian coordinate system is defined with coordinates (x,y,z), with unit vectors  $(\hat{i},\hat{j},\hat{k})$ , and with the y axis parallel to each wire. Each wire is approximated as infinitely long and of negligible thickness. The two planes of wires are located at z=0 and z=d=|d|. Each wire located at the z=0 plane carries a current I=|I|, which flows in the  $\hat{j}$  direction, and each wire located at the z=d plane carries a current -I, which flows in the  $-\hat{j}$ . Two adjacent wires on the same plane are separated by a distance S, which is the spatial period of the configuration.

The magnetic field produced by two wires, one located at coordinates (0, y, 0) (i.e., coin-

### AIP Publishing

This is the author's peer reviewed, accepted manuscript. However, the online version of record will be different from this version once it has been copyedited and typeset

PLEASE CITE THIS ARTICLE AS DOI: 10.1063/5.0030215

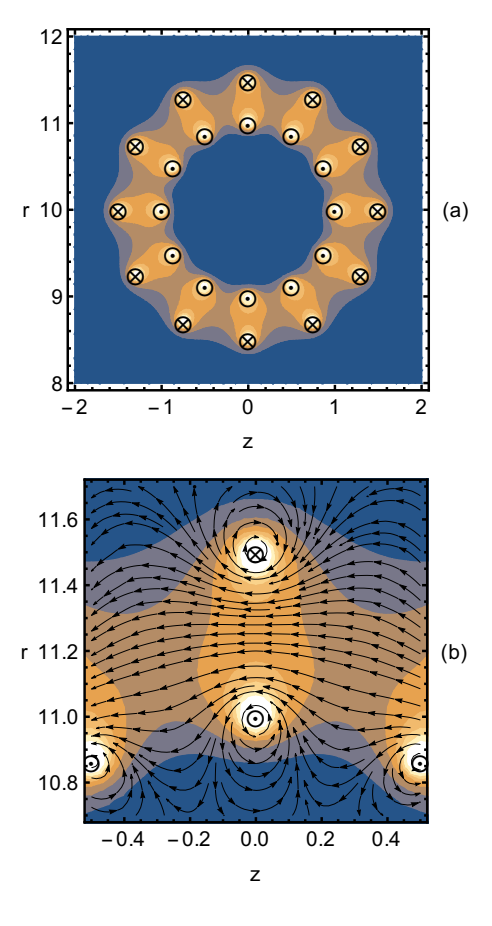


FIG. 1. Example of a purely magnetic applied field that would be produced by an artificially structured boundary for confining an effectively unmagnetized plasma. The field is axisymmetric, and the axis of symmetry (not shown) is coincident with the z axis of a cylindrical coordinate system. A contour plot of the field magnitude on an r-z plane is shown in (a), and a close-up view is shown in (b). The transitions between different colors occur at contours of constant magnetic field strength. The lines with arrows in (b) indicate the local direction of the magnetic field. There are 24 magnetic coils, with the location of each indicated by a circle with either a central dot (indicating current flow "out of the page") or a cross (indicating current flow "into the page").

This is the author's peer reviewed, accepted manuscript. However, the online version of record will be different from this version once it has been copyedited and typeset PLEASE CITE THIS ARTICLE AS DOI: 10.1063/5.0030215

-I-I-I-I-I-I-I-I-I0 0 0 0 0 0 0 0 0 8 8 8 8 8 8 8 8 8  $\rightarrow$ Χ Ι Ι Ι Ι Ι Ι Ι Ι Ι

FIG. 2. Planar model of an artificially structured boundary. The model consists of two sets of parallel wires, with one set located on the z=0 plane of a Cartesian coordinate system, and the other set located on the z=d=|d| plane. A confined plasma would be located at z< d. Each wire in the z=0 plane would be immersed within the plasma and would carry a current I=|I| in the positive  $\hat{j}$  direction ("into the page"). Each wire in the z=d plane would not be immersed within the plasma and would carry a current -I in the negative  $\hat{j}$  direction. Adjacent wires in the same plane are separated by a distance S.

cident with the y axis) and the other at coordinates (0, y, d) is given by

$$\mathbf{B}_{0}(x,y,z) = \frac{\mu_{0}I}{2\pi} \left[ \left( \frac{z}{x^{2}+z^{2}} - \frac{z-d}{x^{2}+(z-d)^{2}} \right) \hat{\mathbf{i}} - \left( \frac{x}{x^{2}+z^{2}} - \frac{x}{x^{2}+(z-d)^{2}} \right) \hat{\mathbf{k}} \right].$$
(3)

Here,  $\mu_0$  is the permeability of free space, and SI units are used.

Each plane of wires extends to  $\pm \infty$  in the x dimension. The magnetic field is evaluated as the superposition of the fields of all pairs of wires:

$$\mathbf{B}(x, y, z) = \sum_{k=-\infty}^{\infty} \mathbf{B}_0 (x - kS, y, z)$$
$$= \frac{1}{2} B_m \boldsymbol{\beta}, \tag{4}$$

where  $B_m = \mu_0 I/S$ ,  $\boldsymbol{\beta} = \beta_x \hat{\boldsymbol{i}} + \beta_y \hat{\boldsymbol{j}} + \beta_z \hat{\boldsymbol{k}}$ ,  $\beta_y = 0$ ,

$$\beta_{x} = \frac{1}{\coth(2\pi z_{n}) - \cos(2\pi x_{n}) \operatorname{csch}(2\pi z_{n})} - \frac{1}{\coth[2\pi (z_{n} - d_{n})] - \cos(2\pi x_{n}) \operatorname{csch}[2\pi (z_{n} - d_{n})]},$$
(5)

### AP Publishing

PLEASE CITE THIS ARTICLE AS DOI: 10.1063/5.0030215

This is the author's peer reviewed, accepted manuscript. However, the online version of record will be different from this version once it has been copyedited and typeset

and

$$\beta_{z} = \frac{1}{\cot(2\pi x_{n}) - \csc(2\pi x_{n}) \cosh(2\pi z_{n})} - \frac{1}{\cot(2\pi x_{n}) - \csc(2\pi x_{n}) \cosh[2\pi (z_{n} - d_{n})]}.$$
 (6)

Here,  $x_n = x/S$ ,  $z_n = z/S$ , and  $d_n = d/S$ . Figures 3 and 4 show plots of the magnetic field given by Eq. (4).

For  $d \ll S$  the magnetic field strength  $B = |\mathbf{B}|$  varies significantly as a function of x at z = d/2, midway between the two planes of current carrying wires. For  $d \gtrsim S$ , the magnetic field near z = d/2 is relatively uniform, approaching the value  $B_m$  in the limit  $d \gg S$ .

The magnetic field strength decreases precipitously over a distance of a few spatial periods away from the artificially structured boundary. For example, for  $d \geq S$ , if the magnetic field strength is  $\sim 1$  T at z=d/2, the magnetic field strength is approximately  $10^{-14}$  T at z=-5S. Therefore, it is possible for a charged particle of a given kinetic energy to be effectively free of the magnetic field if located at  $z \lesssim -5S$  and magnetized if located at  $z \approx d/2$ . The dimensions of a plasma confined by an artificially structured boundary similar to that in Fig. 2 would be large compared to the spatial period of the applied field, and the plasma would be effectively unmagnetized, except near the edge of the plasma.

In Fig. 3b, two magnetic field lines are shown. (The other lines with arrows are not referred to as field lines, which are continuous, because the other lines may be shown as being discontinuous to avoid overcrowding of lines.) One magnetic field line encircles the wire and the other magnetic field line does not. A separatrix occurs at the transition between field lines that do and do not encircle the wire. The minimum distance of closest approach between the separatrix and the wire depends on the value of  $d_n = d/S$ . By varying the value of  $d_n$ , it is found that, for  $d \ge 0.5S$ , the minimum distance of closest approach between the separatrix and the wire is between 0.10S and 0.12S. In Fig. 3b, with  $d_n = 1$ , the separatrix approaches most closely to the wire at the normalized coordinates  $(x_n = 0, y_n, z_n = 0.11)$ , where  $y_n = y/S$ .

### IV. PARTICLE REFLECTION

A classical trajectory Monte Carlo simulation is used for following the trajectories of charged particles that approach the artificially structured boundary in Fig. 2. The governing

### AP

This is the author's peer reviewed, accepted manuscript. However, the online version of record will be different from this version once it has been copyedited and typeset.

PLEASE CITE THIS ARTICLE AS DOI: 10.1063/5.0030215

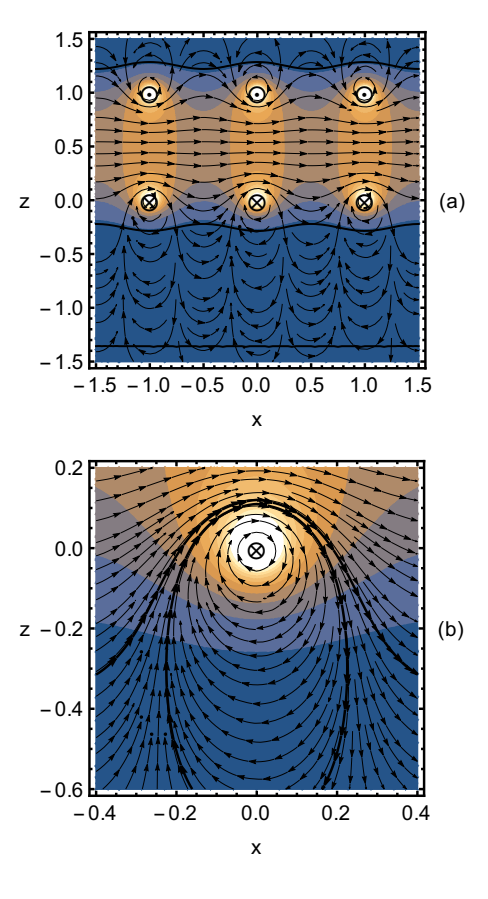


FIG. 3. Magnetic field produced by the artificially structured boundary in Fig. 2, with spatial dimensions normalized by the spatial period S and with d=1. Three spatial periods are shown in (a), and a close-up view is shown in (b). The lines with arrows indicate the local direction of the magnetic field. The transitions between different colors occur at contours of constant magnetic field strength B=|B|. The solid lines without arrows in (a) also occur at contours of constant magnetic field strength. The magnetic field strength at the solid line near the bottom of (a) is smaller than at the other two solid lines by a factor of  $10^{-3}$ . The two solid lines with arrows in (b) represent magnetic field lines that do and do not encircle a wire, respectively. A separatrix occurs at the transition between field lines that do and do not encircle the wire.

# This is the author's peer reviewed, accepted manuscript. However, the online version of record will be different from this version once it has been copyedited and typeset

PLEASE CITE THIS ARTICLE AS DOI: 10.1063/5.0030215

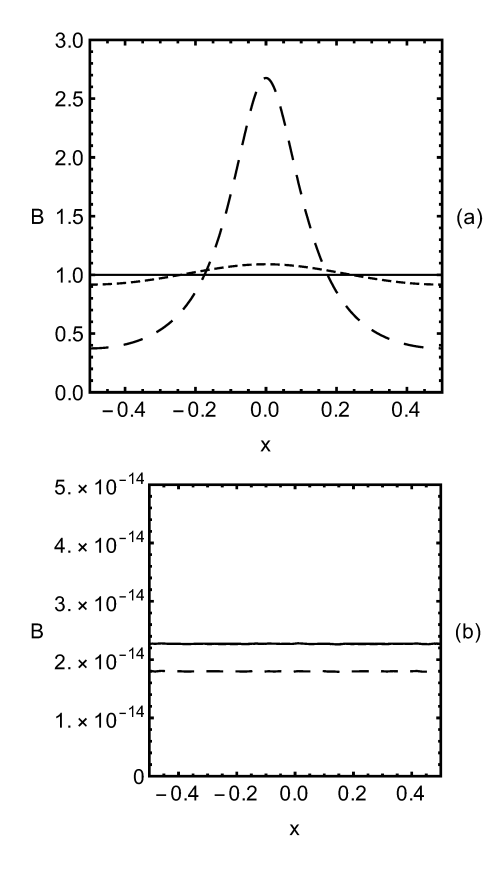


FIG. 4. Magnitude of the magnetic field produced by the artificially structured boundary in Fig. 2, with spatial dimensions normalized by the spatial period S and with the magnetic field normalized by  $B_m$ . The magnetic field strengths at z=d/2 (a) and at z=-5S (b) are plotted, with d=4S (solid line), d=S (short-dash line), and d=S/4 (long-dash line). Two of the lines overlap in (b).

equations solved by the simulation consist of three classical equations of motion and six initial conditions. The equations of motion to be solved consist of the three components of Newton's second law with a magnetic Lorentz force,  $m\mathbf{a} = q\mathbf{v} \times \mathbf{B}$ . Here, m and q are the mass and charge of a particle,  $\mathbf{v} = \mathbf{r}'(t)$  and  $\mathbf{a} = \mathbf{r}''(t)$  are the particle's velocity and acceleration, with the particle's position  $\mathbf{r}$  being a function of time t, and  $\mathbf{B}$  is the magnetic field through which the particle travels. Normalized governing equations are to be used, such that the

### Publishing Publishing

This is the author's peer reviewed, accepted manuscript. However, the online version of record will be different from this version once it has been copyedited and typeset

PLEASE CITE THIS ARTICLE AS DOI: 10.1063/5.0030215

results are more broadly applicable. Four normalization factors are chosen to be the mass m and charge q of a particle, the spatial period S of the magnetic field, and the classical kinetic energy of a particle,  $K = (1/2)mv^2$ , which is a conserved quantity when only a magnetic force is present. Other normalization factors that are needed are obtained using dimensional analysis. Each normalized quantity is dimensionless and is written using the same symbol as its unnormalized counterpart, except with a subscript n attached. The normalized quantities used here are related to unnormalized quantities as follows:  $\mathbf{r}_n = \mathbf{r}/S$ ,  $\mathbf{v}_n = \mathbf{v}\sqrt{m/K}$ ,  $\mathbf{a}_n = \mathbf{a}mS/K$ ,  $t_n = t(1/S)\sqrt{K/m}$ , and  $\mathbf{B}_n = \mathbf{B}qS/\sqrt{mK}$ . Also,  $m_n = q_n = K_n = S_n = 1$ . Solving for  $\mathbf{a}$ ,  $\mathbf{v}$ , and  $\mathbf{B}$ , and substituting into the equations of motion gives normalized equations of motion,  $\mathbf{a}_n = \mathbf{v}_n \times \mathbf{B}_n$ . Referring to Eq. (4), the normalized magnetic field can be written as

$$\boldsymbol{B}_{n}(x_{n}, y_{n}, z_{n}) = \frac{\operatorname{sgn}(q)}{\sqrt{2}r_{mn}}\boldsymbol{\beta},\tag{7}$$

where  $\operatorname{sgn}(q) = q/|q|$  and  $r_{mn} = r_m/S = \sqrt{2mK}/(|q|B_mS)$ . Here,  $r_m$  is a positive parameter that would equal the Larmor radius for a particle located within a uniform magnetic field of magnitude  $B_m$  and having kinetic energy K associated with circular motion.

The normalized equations of motion are

$$x_n''(t_n) = \frac{\text{sgn}(q)}{\sqrt{2}r_{mn}} \left[ y_n'(t_n)\beta_z - z_n'(t_n)\beta_y \right], \tag{8}$$

$$y_n''(t_n) = \frac{\operatorname{sgn}(q)}{\sqrt{2}r_{mn}} \left[ z_n'(t_n)\beta_x - x_n'(t_n)\beta_z \right],$$
 (9)

and

$$z_n''(t_n) = \frac{\text{sgn}(q)}{\sqrt{2}r_{mn}} \left[ x_n'(t_n)\beta_y - y_n'(t_n)\beta_x \right].$$
 (10)

The functional dependence,  $\beta = \beta [x_n(t_n), y_n(t_n), z_n(t_n)]$ , is not shown in Eqs. (8) to (10) for brevity. Equations (8) to (10) are solved numerically. An indication of the numerical inaccuracy of a solution is the change of a particle's normalized kinetic energy, which is a conserved quantity. Each particle's normalized kinetic energy changed away from a value of 1 by an amount that was typically less than 0.001% for each solution reported here.

Some of the initial conditions are sampled from distribution functions, by using analytical sampling expressions. For example, suppose that  $f(\theta_0)$  is a distribution function, and values of  $\theta_0$  are to be sampled. The relation,

$$R_{\theta} = \frac{\int_{\theta_{l}}^{\theta_{0}} f_{\theta}(\theta) d\theta}{\int_{\theta_{l}}^{\theta_{l}} f_{\theta}(\theta) d\theta},\tag{11}$$

This is the author's peer reviewed, accepted manuscript. However, the online version of record will be different from this version once it has been copyedited and typeset PLEASE CITE THIS ARTICLE AS DOI: 10.1063/5.0030215

is solved analytically to obtain a sampling expression,  $\theta_0 = \theta_0(R_\theta)$ , where  $\theta_l$  and  $\theta_u$  are lower and upper limits for the possible values of  $\theta_0$ . Hereafter, the symbol R with a subscript (e.g.,  $R_\theta$ ) denotes an independent random number that is equally likely to have any value between 0 and 1.

The initial normalized spatial coordinates used are

$$x_n(0) = x_{0n} = R_x - 0.5, (12)$$

$$y_n(0) = y_{0n} = R_y - 0.5, (13)$$

$$z_n(0) = z_{0n} = -5. (14)$$

In the x and y dimensions, the initial coordinates are randomly sampled over distances equal to one spatial period of the magnetic field. Such sampling in the x dimension is consistent with considering the spatial period of the magnetic field in the x dimension to be much smaller than the spatial variation of a source of incident particles. The value used for  $y_{0n}$  is unimportant in this Sec. IV, because the magnetic field has no spatial variation in the y dimension. The magnitude of the initial coordinate in the z dimension is chosen to be large enough for the effect of the magnetic field on a trajectory to be negligible near  $z_{0n}$ .

The initial normalized velocity components are written as

$$v_{xn}(0) = v_{0xn} = v_{0n} \sin \theta_0 \cos \phi_0, \tag{15}$$

$$v_{yn}(0) = v_{0yn} = v_{0n} \sin \theta_0 \sin \phi_0, \tag{16}$$

$$v_{zn}(0) = v_{0zn} = v_{0n}\cos\theta_0. \tag{17}$$

Here,  $(v_{0n}, \theta_0, \phi_0)$  are spherical coordinates in velocity space. The initial normalized speed of each particle is  $v_{0n} = \sqrt{2}$ , because the initial kinetic energy of each particle is  $K_n = 1 = m_n v_{0n}^2/2$ , and the normalized mass of a particle is  $m_n = 1$ .

The possible values of  $\phi_0$  are limited to  $0 \le \phi_0 < 2\pi$ . The value of  $\theta_0$  is limited to  $0 \le \theta_0 < \theta_{\rm max}$  with  $\theta_{\rm max} < \pi$ . Particles with  $\theta_{\rm max} > \pi/2$  would initially travel in the  $-\hat{k}$  direction, which is away from the artificially structured boundary. Also, particles that would initially travel nearly parallel to the z=0 plane could make the computation unmanageable. Such particles can be excluded by selecting a value for  $\theta_{\rm max}$  that is slightly less than  $\pi/2$ . Here in Sec. IV, the value  $\theta_{\rm max} = 0.9\pi/2$  is used, and incident particles are considered to

### A Publishing

PLEASE CITE THIS ARTICLE AS DOI: 10.1063/5.0030215

This is the author's peer reviewed, accepted manuscript. However, the online version of record will be different from this version once it has been copyedited and typeset

follow a monoenergetic isotropic velocity distribution function,

$$f(v_{0n}, \theta_0, \phi_0) = f_0 \delta(v_{0n} - \sqrt{2}) f_{\theta}(\theta_0) f_{\phi}(\phi_0).$$
(18)

Here,  $f_0$  is a normalization constant,  $\delta$  is the Dirac delta function, and the (unnormalized) angle distribution functions are  $f_{\theta}(\theta_0) = \sin \theta_0$ , and  $f_{\phi}(\phi_0) = 1$ . The associated sampling expressions are

$$\phi_0 = 2\pi R_\phi,\tag{19}$$

and

$$\theta_0 = \arccos\left[1 - R_\theta + R_\theta \cos\left(\theta_{\text{max}}\right)\right],\tag{20}$$

where the limits of integration,  $\theta_l = 0$  and  $\theta_u = \theta_{\text{max}}$ , are used in Eq. (11) for obtaining Eq. (20). Substitution of the sampling expressions, Eqs. (19) and (20), into the expressions for the velocity components, Eqs. (15) - (17), gives

$$v_{0xn} = \sqrt{2 - 2\left[1 - R_{\theta} + R_{\theta}\cos(\theta_{\text{max}})\right]^2}\cos(2\pi R_{\phi}),$$
 (21)

$$v_{0yn} = \sqrt{2 - 2\left[1 - R_{\theta} + R_{\theta}\cos\left(\theta_{\text{max}}\right)\right]^2} \sin\left(2\pi R_{\phi}\right),$$
 (22)

$$v_{0zn} = \sqrt{2} \left[ 1 - R_{\theta} + R_{\theta} \cos \left(\theta_{\text{max}}\right) \right]. \tag{23}$$

Each simulated trajectory is discontinued either when the particle reaches  $z_n > d_n$  (and is considered to be lost) or when the particle reaches  $z_n < z_{0n}$  (after being reflected by the magnetic field). Also, if a maximum normalized time,  $t_{n,\max} = 2700/\sqrt{2}$ , is reached, the particle is considered to become magnetically trapped. That is, if a simulated particle travels (at normalized speed  $\sqrt{2}$ ) a normalized path length that reaches 2700 spatial periods, the trajectory is discontinued, and the particle is considered to have become magnetically trapped.

Figure 5 shows plots of 1000 trajectories that result from a simulation. The value,  $r_{mn} = 0.01$ , was used, and all particles are reflected by the magnetic field. A positive sign of charge, sgn(q) = 1, was used. It should be noted, however, that statistically averaged results from the simulation do not depend on the value of sgn(q), because  $x_{0n}$  is sampled uniformly over one spatial period.

Figure 6 shows the conditions found for all incident particles to be reflected for various values of  $d_n$ . The simulations are the same as for Fig. 5, except that different values for

This is the author's peer reviewed, accepted manuscript. However, the online version of record will be different from this version once it has been copyedited and typeset

FIG. 5. Results for a simulation with  $r_{mn}=0.01$ . Shown are parametric plots of trajectories over a region with multiple spatial periods (a) and over a region with a single spatial period (b). The close-up view of one spatial period shown in (b) has the location of a current-carrying wire indicated by a circle with a cross. Individual trajectory lines may not be distinguishable as a result of overlapping lines. All particles start under effectively unmagnetized conditions at  $z_n=-5$ , and all particles reach  $z_n<-5$  and are considered to be reflected by the magnetic field. Some reflected particles enter a magnetic cusp, follow the separatrix, and exit a different magnetic cusp.

 $d_n$  and  $r_{mn}$  are used. To determine the conditions,  $d_n$  was chosen to have values that are multiples of 1, except one value was chosen to be 0.5, and  $r_{mn}$  was chosen to have values that are multiples of 0.1. For all particles to be reflected in a simulation, it was found that the value of  $r_{mn}$  had to satisfy the approximate condition,  $r_{mn} < 0.5d_n$ . Based on the values of  $d_n$  used  $(0.5 \le d_n \le 10)$  for Fig. 6, the condition,  $r_{mn} < 0.5d_n$ , is expected to be applicable for  $d_n \ge 0.5$ . No particles became magnetically trapped (i.e., no trajectories reached the maximum normalized time  $t_{n,\max}$ ).

### V. MAGNETIC PLASMA EXPULSION

An electrical coil that produces a magnetic plasma expulsion field is now considered to be added at the x=0 plane of the artificially structured boundary illustrated in Fig. 2. The electrical coil is treated as a single-turn rectangular current loop of wire, which has an infinitesimal thickness. The placement of the coil is illustrated in Fig. 7. Two sides of the loop are of length 2u and are coincident with two infinite-length wires located at

This is the author's peer reviewed, accepted manuscript. However, the online version of record will be different from this version once it has been copyedited and typeset

### 3.0 2.5 2.0 r<sub>mn</sub> 1.5 1.0 0.5 0.0 2 3 4 5 6 $d_n$

FIG. 6. The values of  $r_{mn}$  in multiples of 0.1 for which no losses occur (at smaller  $r_{mn}$  values indicated by green dots) or one or more losses occur (at larger  $r_{mn}$  values indicated by black dots). The line is a plot of  $r_{mn} = 0.5d_n$ . The particles start effectively unmagnetized at  $z_n = -5$ , and each trajectory is discontinued when the particle is reflected (by reaching  $z_n < -5$ ) or when the particle is considered to be lost (by reaching  $z_n > d_n$ ). The values of  $d_n$  are multiples of 1, except one value at  $d_n = 0.5$ .

coordinates (0, y, 0) and (0, y, d). The other two sides of the loop are of length d and are located at coordinates  $(0, u, 0 \le z \le d)$  and  $(0, -u, 0 \le z \le d)$ . The current carried by the rectangular current loop is considered to be cI, where c is a chosen constant, and I is the magnitude of the current carried by one of the infinite-length wires. The direction of the loop's current is such that each coincident segment of the loop and infinite-length wire have opposing currents. In the work presented here, the value c=1 is used, resulting in an equivalent current path that is shown in Fig. 7b. The magnetic field strength diverges along the equivalent current path, which is infinitesimally thin. For monoenergetic particles incident from  $z_n = -5$ , a particle-free volume may be expected to exist in the vicinity of the equivalent current path. Also, by using the value c=1, the current in the magnetic expulsion coil can serve as the current feed between two connected magnetic confinement coils modeled here as infinite-length wires. Therefore, the three coils can be replaced by an equivalent single coil that carries a current along the path illustrated in Fig. 7b.

This is the author's peer reviewed, accepted manuscript. However, the online version of record will be different from this version once it has been copyedited and typeset

PLEASE CITE THIS ARTICLE AS DOI: 10.1063/5.0030215

↑ у

FIG. 7. Addition of a magnetic plasma expulsion coil between two infinite-length wires (a), and the equivalent current path with c=1 (b). The magnetic plasma expulsion coil is modeled as a rectangular current loop with current cI, where c is a chosen constant. The rectangular current loop is located between two infinite-length wires in the x=0 plane of the artificially structured boundary shown in Fig. 2. The wire that forms the rectangular current loop is treated as being infinitesimally thin, and two sides of the loop are treated as being coincident with the infinitelength wires over a distance 2u. The other two sides of the loop, each of length d, are parallel to the z axis.

The current loop produces a magnetic plasma expulsion field that is superimposed on the magnetic plasma confinement field given by Eq. (4). For convenience, the total magnetic field is written as

$$\boldsymbol{B}(x,y,z) = \frac{1}{2} B_m \left( \boldsymbol{\beta} + \boldsymbol{\beta}_e \right), \tag{24}$$

where  $\beta_e$  is defined such that  $B_m\beta_e/2$  is the magnetic field produced by the rectangular current loop. A closed-form expression for the field of a rectangular current loop is obtained from Ref. 32. For the current loop in Fig. 7, the components of  $\beta_e$  can be written as

$$\beta_{ex} = -\frac{c}{2\pi} \left[ \frac{z_n}{r_{1n} (r_{1n} - y_n - u_n)} + \frac{y_n + u_n}{r_{1n} (r_{1n} - z_n)} - \frac{z_n - d_n}{r_{2n} (r_{2n} - y_n - u_n)} - \frac{y_n + u_n}{r_{2n} (r_{2n} - z_n + d_n)} - \frac{z_n}{r_{3n} (r_{3n} - y_n + u_n)} - \frac{y_n - u_n}{r_{3n} (r_{3n} - z_n)} + \frac{z_n - d_n}{r_{4n} (r_{4n} - y_n + u_n)} + \frac{y_n - u_n}{r_{4n} (r_{4n} - z_n + d_n)} \right],$$

$$\beta_{ey} = \frac{cx_n}{2\pi} \left[ \frac{1}{r_{1n} (r_{1n} - z_n)} - \frac{1}{r_{2n} (r_{2n} - z_n + d_n)} \right]$$
(25)

This is the author's peer reviewed, accepted manuscript. However, the online version of record will be different from this version once it has been copyedited and typeset

 $-\frac{1}{r_{3n}(r_{3n}-z_n)} + \frac{1}{r_{4n}(r_{4n}-z_n+d_n)}\right],$  (26)

$$\beta_{ez} = \frac{cx_n}{2\pi} \left[ \frac{1}{r_{1n} (r_{1n} - y_n - u_n)} - \frac{1}{r_{2n} (r_{2n} - y_n - u_n)} - \frac{1}{r_{3n} (r_{3n} - y_n + u_n)} + \frac{1}{r_{4n} (r_{4n} - y_n + u_n)} \right],$$
(27)

where

$$r_{1n} = \sqrt{z_n^2 + (y_n + u_n)^2 + x_n^2},$$
(28)

$$r_{2n} = \sqrt{(z_n - d_n)^2 + (y_n + u_n)^2 + x_n^2},$$
(29)

$$r_{3n} = \sqrt{z_n^2 + (y_n - u_n)^2 + x_n^2},$$
(30)

$$r_{4n} = \sqrt{(z_n - d_n)^2 + (y_n - u_n)^2 + x_n^2},$$
(31)

and  $u_n = u/S$ .

A magnetic plasma expulsion field superimposed on the field given by Eq. (4) is shown in Fig. 8. The spatial dimensions are normalized by the spatial period S, and the following parameter values are used for the plot:  $d_n = 1$ , c = 1,  $u_n = 0.05$ , and  $z_n = d_n/2$ . Magnetic plasma expulsion is described in detail in Refs. 13 and 15. Without the magnetic plasma expulsion field present, the magnetic field would be approximately straight and parallel to the x axis. With the magnetic plasma expulsion field present, there are two regions in Fig. 8 that would remain free of particles if particles only followed the field line.

A classical trajectory Monte Carlo simulation is carried out in the same way as in Sec. IV, except that the magnetic plasma expulsion field is included by making the replacement  $\beta \to \beta + \beta_e$  in the equations of motion, Eqs. (8) to (10). The value, c = 1, is chosen without an optimization process.

Figure 9 shows the conditions found for all incident particles to be reflected for various values of  $u_n$ . The simulations are the same as for Fig. 6, except that  $\theta_{\text{max}} = 0$  is used to maximize the number of particles that enter a cusp, follow the separatrix, and encounter the magnetic field distortion introduced by the presence of the magnetic plasma expulsion field. Also,  $d_n = 1$  is used, and various values of  $r_{mn}$  are used. To determine the conditions for all incident particles to be reflected,  $u_n$  was chosen to have values that are multiples of 0.01, and  $r_{mn}$  was chosen to have values that are multiples of 0.001. For all particles to be reflected in a simulation, it was found that  $r_{mn}$  had to have values within a certain range

This is the author's peer reviewed, accepted manuscript. However, the online version of record will be different from this version once it has been copyedited and typeset

0.1 y 0.0 -0.1 -0.2 -0.2 -0.1 0.0 0.1 0.2 x

FIG. 8. Magnetic field produced by the artificially structured boundary in Fig. 2 combined with the rectangular loop in Fig. 7, with spatial dimensions normalized by the spatial period S and with  $d_n = 1$ , c = 1,  $u_n = 0.05$ , and  $z_n = d_n/2$ . The lines with arrows indicate the local direction of the magnetic field. The transitions between different colors occur at contours of constant magnetic field strength. Magnetic plasma expulsion tends to occur in the vicinity of the wire associated with the current loop, indicated by a circle with a cross or a central dot. Without the magnetic plasma expulsion field present, the magnetic field would be approximately straight and parallel to the x axis.

for a given value of  $u_n$ . Outside of the range, at least one particle became magnetically trapped (i.e., a trajectory would reach the maximum normalized time  $t_{n,\max}$ ). The magnetic trapping of particles is attributed to a cross-magnetic-field drift, as discussed in the next section.

### VI. DISCUSSION

The simulations indicate that the applied magnetic field produced by the artificially structured boundary in Fig. 2 can reflect all independently incident particles under certain conditions. For incident particles that follow a monoenergetic isotropic velocity distribution without the magnetic plasma expulsion field present, the condition can be written in terms

This is the author's peer reviewed, accepted manuscript. However, the online version of record will be different from this version once it has been copyedited and typeset

0.015
0.010
0.005
0.000
0.000
0.002
0.004
0.006
0.008
0.10
0.12

Un

FIG. 9. The values of  $r_{mn}$  in multiples of 0.001 for which all 1000 particles would be reflected (small green dots). In some cases, a particle would become magnetically trapped and not leave the vicinity of an infinite-length wire such that  $|x_n(t_{n,\max})| < 0.5$  occurred (medium-sized blue dots) or a particle would become magnetically trapped and moved away from the  $x_n = 0$  plane such that  $|x_n(t_{n,\max})| \geq 0.5$  occurred (large-sized black dots), and the simulation would be discontinued. The value  $d_n = 1$  was used, and none of the particles reached  $z_n > d_n$ . The particles start effectively unmagnetized at  $z_n = -5$ , and the velocity vector of each particle is initially parallel to z axis (with  $\theta_{\max} = 0$ ). A trajectory is discontinued when the particle is reflected (by reaching  $z_n < -5$ ) or when the particle is considered to become magnetically trapped (i.e., the trajectory would reach the maximum normalized time  $t_{n,\max}$ ). The values of  $u_n$  are multiples of 0.01, and the values c = 1 and  $t_{n,\max} = 2700/\sqrt{2}$  were used.

of unnormalized parameters as  $r_m < 0.5d$ , which should be used with  $d \ge 0.5S$ , because smaller values of d were not considered. For a confined plasma with a Maxwellian velocity distribution, the condition can be satisfied by particles other than those in the tail of the distribution by writing the condition as

$$r_{th} \ll 0.5d,\tag{32}$$

where  $r_{th} = \sqrt{mkT/(q^2B_m^2)}$  is the thermal Larmor radius, T is the plasma temperature and k is Boltzmann's constant. The thermal Larmor radius within the magnetic field midway between the planes of wires must be much smaller than one-half of the distance between the

This is the author's peer reviewed, accepted manuscript. However, the online version of record will be different from this version once it has been copyedited and typeset

PLEASE CITE THIS ARTICLE AS DOI: 10.1063/5.0030215

### AIP Publishing

planes of wires.

A charged r

A charged particle that follows a curved magnetic field will drift across the magnetic field in a direction perpendicular to the plane formed by the local field curvature. The cross-magnetic-field drift due to field curvature can consist of two drifts that superimpose. One drift is caused by a gradient of the magnetic field strength and the other is caused by a centrifugal effect. A cross-magnetic-field drift due to field curvature would occur for particles that are magnetized within the axisymmetric magnetic plasma confinement field shown in Fig. 1. However, such a drift would be in the azimuthal direction (either into or out of the page in Fig. 1), in the limit that magnetic field asymmetries are negligible. For the planar model of the magnetic field shown in Fig. 3, the magnetic field has no y dependence, and a curvature drift would be in the y direction (either into or out of the page in Fig. 3).

The magnetic plasma expulsion field considered here has a y dependence, as indicated in Fig. 8, and a curvature drift can occur due to the presence of the magnetic plasma expulsion field. As indicated in Fig. 9, for some simulations, a trajectory reached a maximum normalized time without the particle being reflected (by reaching  $z_n < z_{0n}$ ) and without the particle being lost (by reaching  $z_n > d_n$ ). Simulation results indicate that such cases only occurred while the magnetic plasma expulsion field is present. Evidently, the cross-magnetic-field drift that a plasma particle experiences while passes through the magnetic expulsion region can cause magnetic trapping to occur.

Figure 10 shows an illustration of an idealized magnetic field line associated with magnetic plasma expulsion. The line was drawn using four identical segments that are rotated and translated, assuming that horizontal mirror-image symmetry occurs about the horizontal center of the drawing for the magnetic field. Two of the segments would be associated with a curvature drift step that is exactly equal in magnitude and opposite in direction as the curvature drift step associated with the other two segments, for single-particle motion in the guiding-center approximation. It may be possible for the net cross-magnetic-field drift of a plasma particle that passes through the magnetic expulsion region to be negligible with an optimized design of the magnetic plasma expulsion field, such that magnetic trapping of particles due to a curvature drift is minimized or negligible.

When plasma particles become magnetically trapped, cross-magnetic-field transport can be expected to occur that eventually results in the particles being lost or being released back into the effectively unmagnetized plasma region. The rate at which particles are lost

This is the author's peer reviewed, accepted manuscript. However, the online version of record will be different from this version once it has been copyedited and typeset

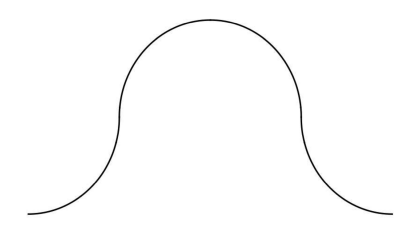


FIG. 10. Model magnetic field line for considering the cross-magnetic-field drift of a plasma particle that passes through the magnetic expulsion region.

is expected to be limited by the slower of two rates, consisting of (1) the net rate at which particles become magnetically trapped and (2) the fastest rate at which magnetically trapped particles are lost due to cross-magnetic-field transport. The results in Fig. 9 indicate that particles with kinetic energies outside of a certain range will become magnetically trapped for the magnetic plasma expulsion field model that was used. Thus, incident particles that follow a Maxwellian velocity distribution may become magnetically trapped with too high or too low of a kinetic energy. Such a situation warrants an attempt to optimize the design of the magnetic plasma expulsion field, such that the magnetic trapping rate due to the curvature drift is minimized. The best case scenario is one in which classical (collision-based) processes govern both the net rate at which particles become magnetically trapped and the fastest rate at which magnetically trapped particles are lost due to cross-magnetic-field transport.

The planar model considered here may be expected to apply for achieving three-dimensional magnetic confinement of nonmagnetically trapped particles using a configuration such as that shown in Fig. 1, provided that the dimensions of the particle confinement volume are large compared to the separation between adjacent plasma-immersed magnetic coils. An alternative to a toroidal confinement volume, such as that illustrated in Fig. 1, would be an axisymmetric cylindrical confinement volume. Such a confinement configuration would have two point cusps along the axis of symmetry, with one at each axial end, that could be connected to Penning traps with axially varying magnetic fields. Electrostatic equilibria computed for nonneutral plasmas confined in a Penning trap with an axially varying magnetic field indicate the possibility of providing plasma space-charge based confinement involving such Penning traps.<sup>33,34</sup>

This is the author's peer reviewed, accepted manuscript. However, the online version of record will be different from this version once it has been copyedited and typeset

PLEASE CITE THIS ARTICLE AS DOI: 10.1063/5.0030215

### AIA Publishing

### VII. CONCLUSION

A planar model has been developed for an artificially structured boundary that may provide magnetic confinement of nonmagnetically trapped plasma particles. The planar model is applicable in the limit that the dimensions of the particle confinement volume are large compared to the separation between adjacent plasma-immersed magnetic coils. A closed-form expression for the magnetic field is given by Eq. (4). Based on classical trajectory Monte Carlo simulation results, predictions have been made regarding conditions that are suitable (but not necessarily sufficient) for particle confinement to occur, including the effect of superimposing a magnetic plasma expulsion field.

### ACKNOWLEDGMENTS

This material is based upon work supported by the National Science Foundation under Grant No. PHY-1803047.

The data that supports the findings of this study are available within the article. (Computational data displayed in Figs. 6 and 9 consist of numerical values located at tick marks that can be read from each figure.)

<sup>&</sup>lt;sup>1</sup> C. A. Ordonez, J. Appl. Phys. **106**, 024905 (2009).

<sup>&</sup>lt;sup>2</sup> C. A. Ordonez, J. L. Pacheco, and D. L. Weathers, Proceedings of the 47th AIAA/ ASME/SAE/ASEE Joint Propulsion Conference & Exhibit, Paper No. AIAA 2011-6120 (2011).

<sup>&</sup>lt;sup>3</sup> R. M. Hedlof and C. A. Ordonez, *Phys. Plasmas* **26**, 092509 (2019).

<sup>&</sup>lt;sup>4</sup> R. M. Hedlof and C. A. Ordonez, AIP Adv. 7, 115123 (2017).

<sup>&</sup>lt;sup>5</sup> R. M. Hedlof and C. A. Ordonez, AIP Conf. Proc. **1928**, 020003 (2018).

<sup>&</sup>lt;sup>6</sup> J. L. Pacheco, C. A. Ordonez, and D. L. Weathers, *Phys. Plasmas* **19**, 102510 (2012).

<sup>&</sup>lt;sup>7</sup> S. Yoshikawa, *Nucl. Fusion* **13**, 433 (1973).

<sup>&</sup>lt;sup>8</sup> J. C. Sprott and S. C. Prager, *Nucl. Fusion* **25**, 1179 (1985).

<sup>&</sup>lt;sup>9</sup> M. W. Maisel, T. Ohkawa, K. H. Burrell, R. L. Freeman, F. J. Helton, T. H. Jensen, R. J. La Haye, D. O. Overskei, R. Prater, J. M. Rawls, and T. Tamano, *Nucl. Fusion* 25, 1113 (1985).

<sup>&</sup>lt;sup>10</sup> A. Y. Wong, Y. Nakamura, B. H. Quon, and J. M. Dawson, Phys. Rev. Lett. 35, 1156 (1975).

- <sup>11</sup> T. Ohkawa, J. R. Gilleland, T. Tamano, T. Takeda, and D. K. Bhadra, *Phys. Rev. Lett.* 27, 1179 (1971).
- <sup>12</sup> R. W. Schumacher, M. Fukao, A. Y. Wong, R. G. Suchannek, K. L. Lam, and K. Yatsu, *Phys. Rev. Lett.* **46**, 1391 (1981).
- <sup>13</sup> R. E. Phillips and C. A. Ordonez, *Phys. Plasmas* **25**, 012508 (2018).
- <sup>14</sup> B. Lehnert, *Plasma Phys.* **17**, 501 (1975).
- <sup>15</sup> A. Martinez and C. A. Ordonez, AIP Adv. 9, 075209 (2019).
- M. Ahmadi, B. X. R. Alves, C. J. Baker, W. Bertsche, A. Capra, C. Carruth, C. L. Cesar, M. Charlton, S. Cohen, R. Collister, S. Eriksson, A. Evans, N. Evetts, J. Fajans, T. Friesen, M. C. Fujiwara, D. R. Gill, J. S. Hangst, W. N. Hardy, M. E. Hayden, M. E. Hayden, C. A. Isaac, M. A. Johnson, S. A. Jones, S. Jonsell, L. Kurchaninov, N. Madsen, D. Maxwell, J. T. K. McKenna, S. Menary, J. M. Michan, T. Momose, J. J. Munich, K. Olchanski, A. Olin, P. Pusa, C. Ø. Rasmussen, F. Robicheaux, R. L. Sacramento, M. Sameed, E. Sarid, D. M. Silveira, D. M. Starko, G. Stutter, C. So, T. D. Tharp, R. I. Thompson, D. P. van der Werf, and J. S. Wurtele, Nature 561, 211 (2018).
- <sup>17</sup> G. Gabrielse, R. Kalra, W. S. Kolthammer, R. McConnell, P. Richerme, D. Grzonka, W. Oelert, T. Sefzick, M. Zielinski, D. W. Fitzakerley, M. C. George, E. A. Hessels, C. H. Storry, M. Weel, A. Müllers, and J. Walz, *Phys. Rev. Lett.* 108, 113002 (2012).
- N. Kuroda, S. Ulmer, D. J. Murtagh, S. Van Gorp, Y. Nagata, M. Diermaier, S. Federmann, M. Leali, C. Malbrunot, V. Mascagna, O. Massiczek, K. Michishio, T. Mizutani, A. Mohri, H. Nagahama, M. Ohtsuka, B. Radics, S. Sakurai, C. Sauerzopf, K. Suzuki, M. Tajima, H. A. Torii, L. Venturelli, B. Wünschek, J. Zmeskal, N. Zurlo, H. Higaki, Y. Kanai, E. Lodi Rizzini, Y. Nagashima, Y. Matsuda, E. Widmann, and Y. Yamazaki, Nat. Commun. 5, 3089 (2014).
- A. Kellerbauer, M. Amoretti, A. S. Belov, G. Bonomi, I. Boscolo, R. S. Brusa, M. Buchner, V. M. Byakov, L. Cabaret, C. Canali, C. Carraro, F. Castelli, S. Cialdi, M. de Combarieu, D. Comparat, G. Consolati, N. Djourelov, M. Doser, G. Drobychev, A. Dupasquier, G. Ferrari, P. Forget, L. Formaro, A. Gervasini, M. G. Giammarchi, S. N. Gninenko, G. Gribakin, S. D. Hogan, M. Jacquey, V. Lagomarsino, G. Manuzio, S. Mariazzi, V. A. Matveev, J. O. Meier, F. Merkt, P. Nedelec, M. K. Oberthaler, P. Pari, M. Prevedelli, F. Quasso, A. Rotondi, D. Sillou, S. V. Stepanov, H. H. Stroke, G. Testera, G. M. Tino, G. Trenec, A. Vairo, J. Vigue, H. Walters, U. Warring, S. Zavatarelli, and D. S. Zvezhinskij, Nucl. Instrum. Methods Phys. Res., Sect. B

This is the author's peer reviewed, accepted manuscript. However, the online version of record will be different from this version once it has been copyedited and typeset.

PLEASE CITE THIS ARTICLE AS DOI: 10.1063/5.0030215

### **266**, 351 (2008).

- P. Indelicato, G. Chardin, P. Grandemange, D. Lunney, V. Manea, A. Badertscher, P. Crivelli, A. Curioni, A. Marchionni, B. Rossi, A. Rubbia, V. Nesvizhevsky, D. Brook-Roberge, P. Comini, P. Debu, P. Dupre, L. Liszkay, B. Mansoulie, P. Perez, J. M. Rey, B. Reymond, N. Ruiz, Y. Sacquin, B. Vallage, F. Biraben, P. Clade, A. Douillet, G. Dufour, S. Guellati, L. Hilico, A. Lambrecht, R. Guerout, J. P. Karr, F. Nez, S. Reynaud, C. I. Szabo, V. Q. Tran, J. Trapateau, A. Mohri, Y. Yamazaki, M. Charlton, S. Eriksson, N. Madsen, D.P. van der Werf, N. Kuroda, H. Torii, Y. Nagashima, F. Schmidt-Kaler, J. Walz, S. Wolf, P. A. Hervieux, G. Manfredi, A. Voronin, P. Froelich, S. Wronka, and M. Staszczak, Hyperfine Interact. 228, 141 (2014).
- <sup>21</sup> S. S. Patel, S. R. Sun, and C. A. Ordonez, AIP Conf. Proc. **2160**, 070003 (2019).
- <sup>22</sup> K. Flanagan, J. Milhone, J. Egedal, D. Endrizzi, J. Olson, E. E. Peterson, R. Sassella, and C. B. Forest, Phys. Rev. Lett. 125, 135001 (2020).
- <sup>23</sup> E. E. Peterson, D. A. Endrizzi, M. Beidler, K. J. Bunkers, M. Clark, J. Egedal, K. Flanagan, K. J. McCollam, J. Milhone, J. Olson, C. R. Sovinec, R. Waleffe, J. Wallace, and C. B. Forest, Nature Phys. 15, 1095 (2019).
- <sup>24</sup> K. Holste, P. Dietz, S. Scharmann, K. Keil, T. Henning, D. Zschatzsch, M. Reitemeyer, B. Nauschutt, F. Kiefer, F. Kunze, J. Zorn, C. Heiliger, N. Joshi, U. Probst, R. Thuringer, C. Volkmar, D. Packan, S. Peterschmitt, K. -T. Brinkmann, H.-G. Zaunick, M. H. Thoma, M. Kretschmer, H. J. Leiter, S. Schippers, K. Hannemann, and P. J. Klar, Rev. Sci. Instrum. 91, 061101 (2020).
- <sup>25</sup> S. K. Maurya and S. Bhattacharjee, Plasma Res. Express 2, 033001(2020).
- <sup>26</sup> J. R. Conrad, J. L. Radtke, R. A. Dodd, F. J. Worzala, and N. C. Tran, J. Appl. Phys. 62, 4591 (1987).
- <sup>27</sup> P. Machima, M. M. M. Bilek, O. R. Monteiro, and I. G. Brown, Rev. Sci. Instrum. **71**, 3373 (2000).
- <sup>28</sup> R. Limpaecher and K. R. MacKenzie, Rev. Sci. Instrum. 44, 726 (1973).
- <sup>29</sup> A. D. Patel, M. Sharma, N. Ramasubramanian, R. Ganesh, and P. K. Chattopadhyay, Rev. Sci. Instrum. 89, 043510 (2018).
- <sup>30</sup> S. Knappmiller and S. Robertson, Phys. Plasmas 18, 100702 (2011).
- <sup>31</sup> M. Martinez-Sanchez and E. Ahedo, Phys. Plasmas 18, 033509 (2011).



### **ACCEPTED MANUSCRIPT**

This is the author's peer reviewed, accepted manuscript. However, the online version of record will be different from this version once it has been copyedited and typeset. PLEASE CITE THIS ARTICLE AS DOI: 10.1063/5.0030215

S. Hampton, R. A. Lane, R. M. Hedlof, R. E. Phillips, and C. A. Ordonez, AIP Adv. 10, 065320

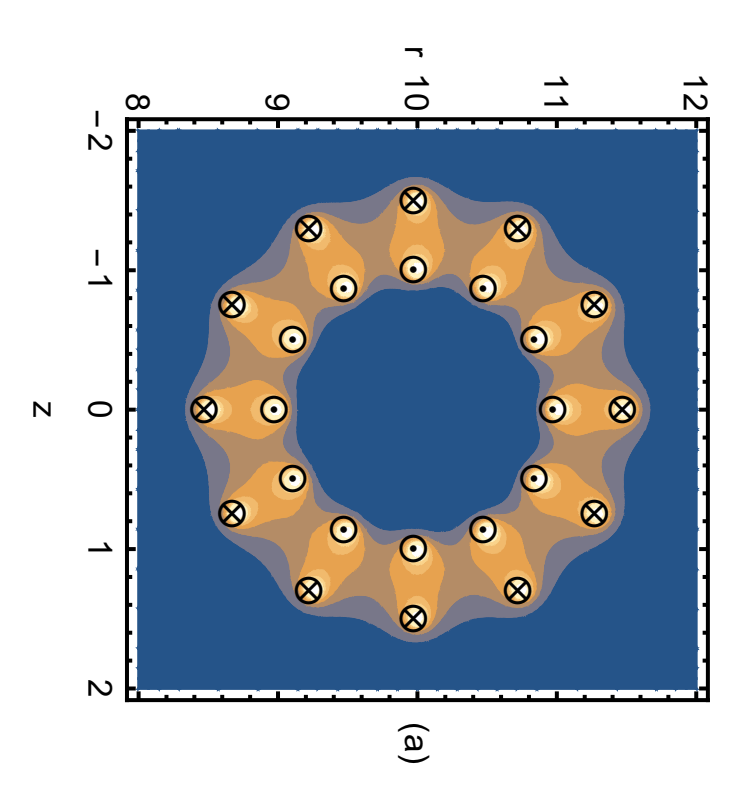
(2020).

R. A. Lane and C. A. Ordonez, Phys. Plasmas 26, 052511 (2019).

R. A. Lane and C. A. Ordonez, J. Phys. B 49, 074008 (2016).

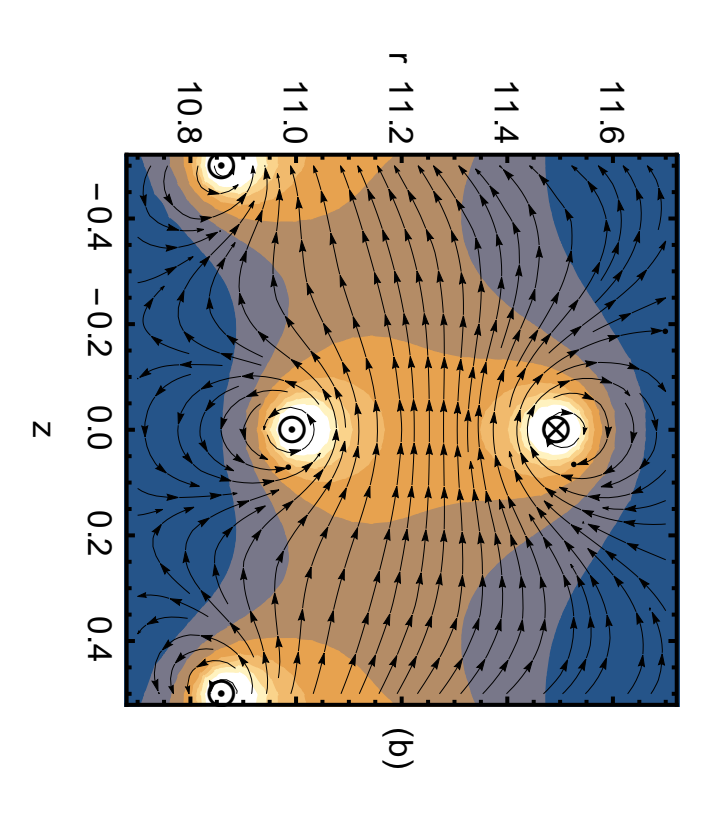


### **ACCEPTED MANUSCRIPT**





### **ACCEPTED MANUSCRIPT**



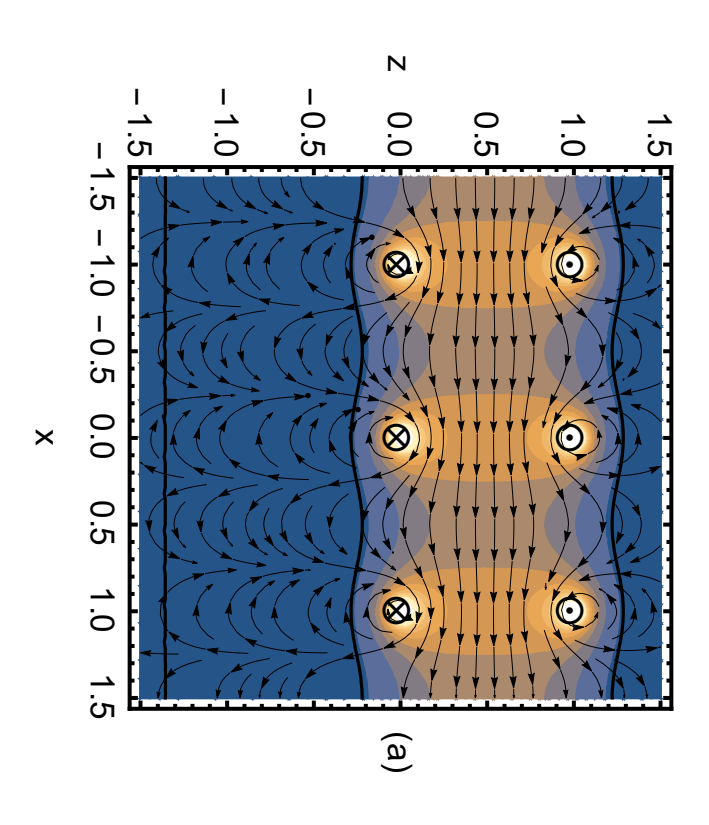


### **ACCEPTED MANUSCRIPT**

$$H \otimes \bigcirc \stackrel{1}{\rightarrow} \rightarrow$$

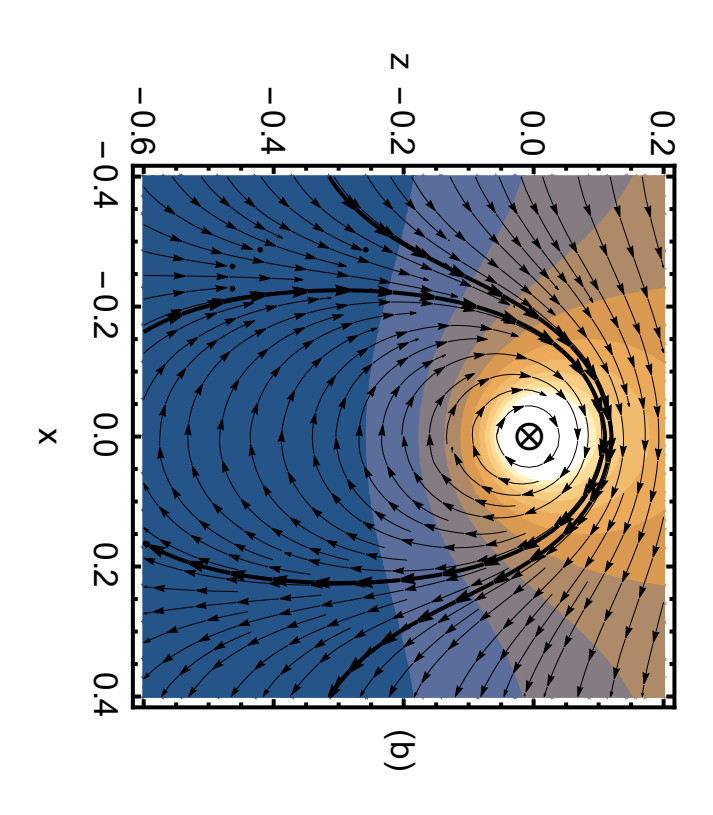


### **ACCEPTED MANUSCRIPT**



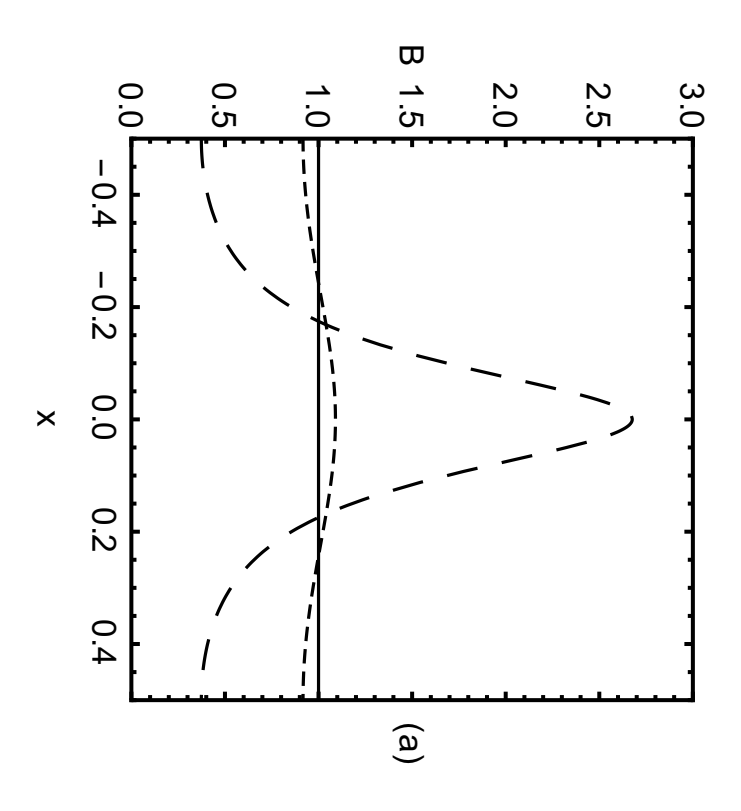


### **ACCEPTED MANUSCRIPT**





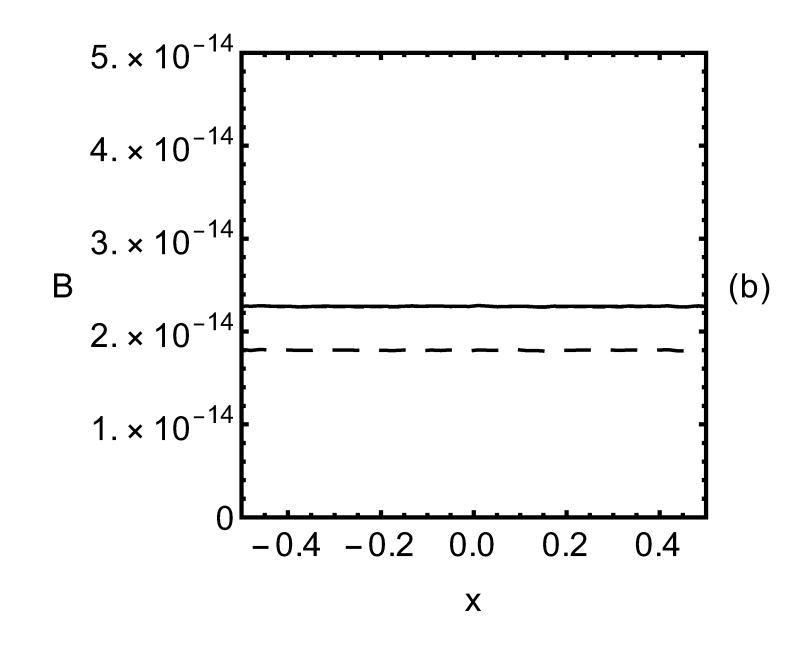
### **ACCEPTED MANUSCRIPT**





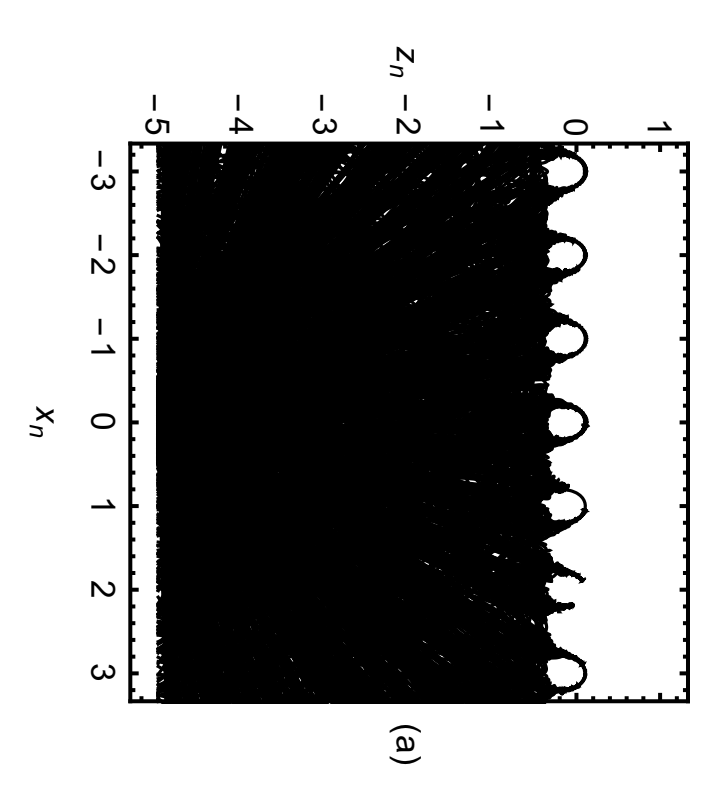
This is the author's peer reviewed, accepted manuscript. However, the online version of record will be different from this version once it has been copyedited and typeset.

PLEASE CITE THIS ARTICLE AS DOI: 10.1063/5.0030215



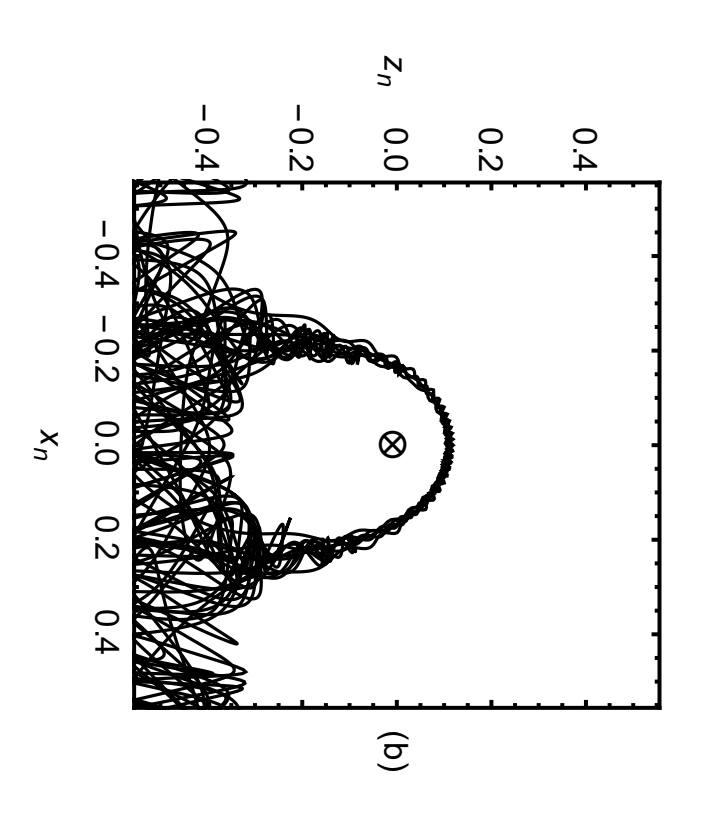


### **ACCEPTED MANUSCRIPT**



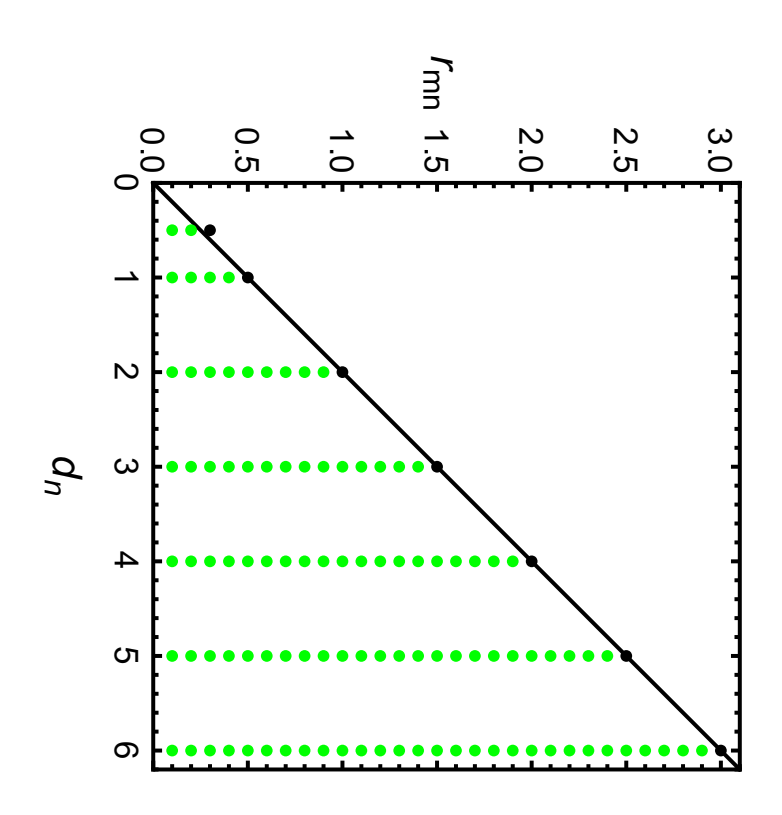


### **ACCEPTED MANUSCRIPT**



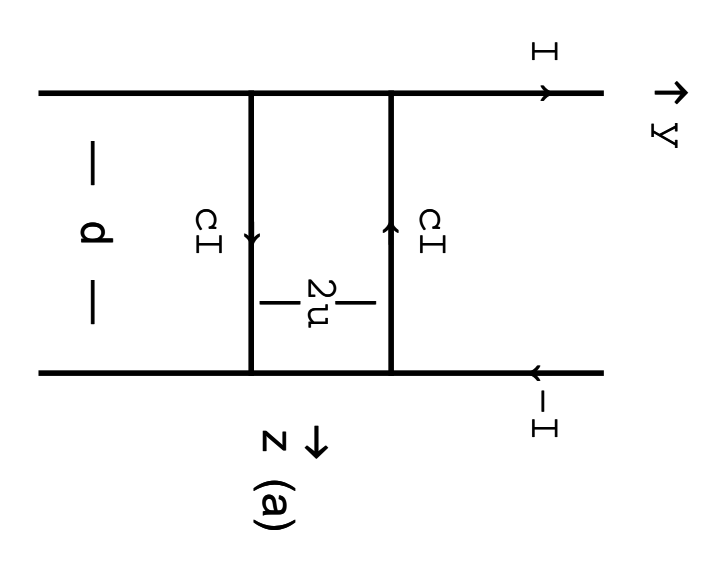


### **ACCEPTED MANUSCRIPT**



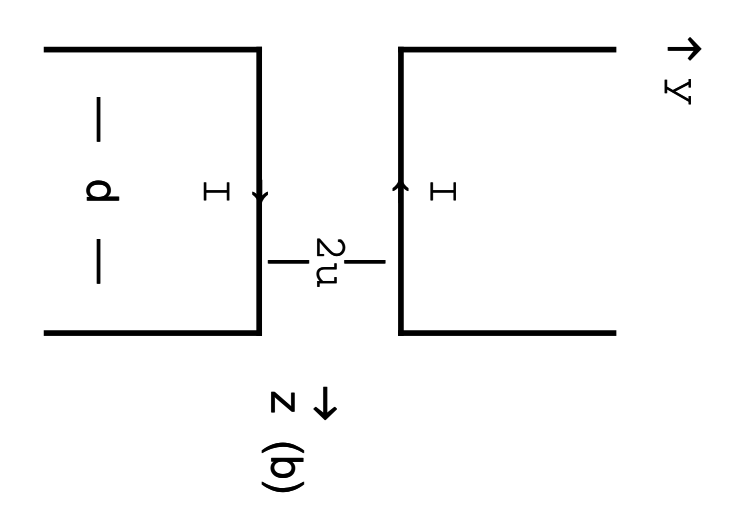


### **ACCEPTED MANUSCRIPT**



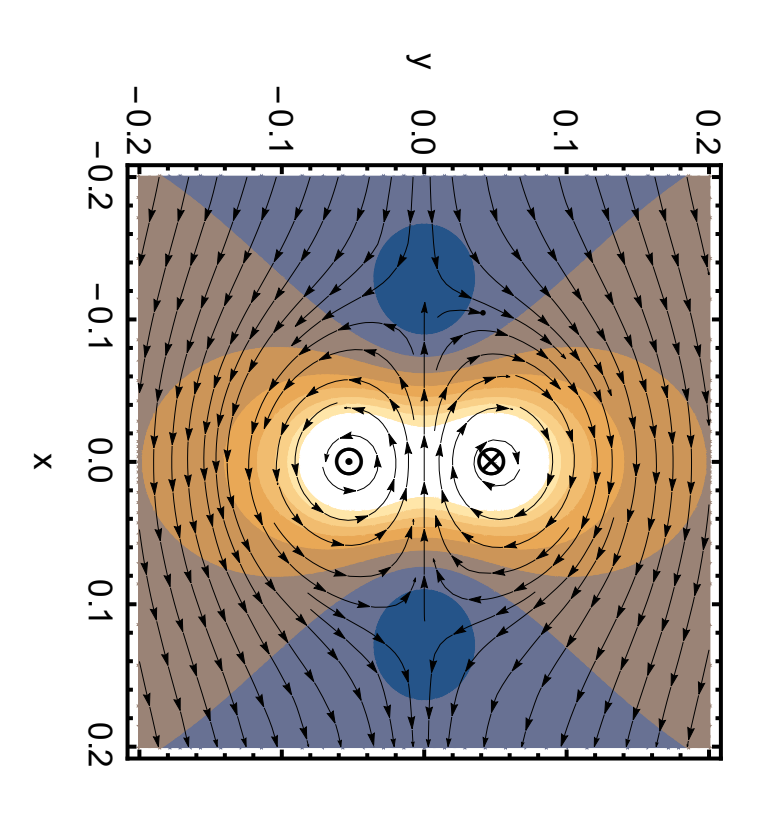


### **ACCEPTED MANUSCRIPT**



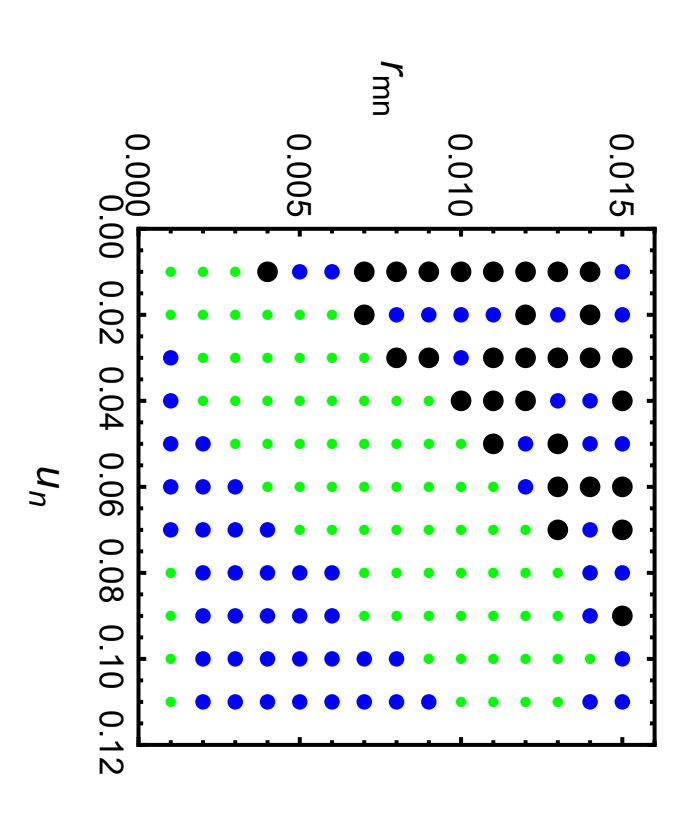


### **ACCEPTED MANUSCRIPT**





### **ACCEPTED MANUSCRIPT**





### **ACCEPTED MANUSCRIPT**

